

Date of publication xxxx 00, 0000, date of current version xxxx 00, 0000.

Digital Object Identifier 10.1109/ACCESS.2017.DOI

Motion Planning and Robust Fault-Tolerant Control of Hybrid UAVs and Biped Robots Team System for Search and Rescue Usage

ABSTRACT In this study, we investigate a motion planning and robust fault-tolerant control of a hybrid UAVs and biped robots team system (URTS) for the purpose of search and rescue (S&R). The system architecture of URTS is proposed at first to illustrate the issues to be addressed in URTS and the relationships between them. The task allocation and path planning problems are first investigated and stated. Next, we focus on the local motion planning problem for UAV flying and robot walking behavior, and then the tracking control problem for UAV and robot. The relationship between local motion planning and tracking control, the transformation of the reference trajectory, is also explored in detail. By converting the dynamics model of UAV and robot into a unified agent model, a design method for an robust H_{∞} decentralized observer-based feedforward-linearized PID fault-tolerant control (FTC) is proposed for the agents in URTS. A novel smoothing signal model of fault signal is embedded into the linearized system to achieve the active FTC through observer estimation. Then, the design of the robust H_{∞} decentralized observer-based feedforward-linearized PID FTC of URTS is transformed into a linear matrix inequality (LMI) -constrained optimization problem which can be solved by a two-step design procedure. With the help of MATLAB LMI Toolbox, the tracking problem of each UAV and robot in URTS is effectively solved. Finally, the simulation results are used to demonstrate the operation of URTS and to verify the effectiveness of the proposed tracking control method under the external disturbance and the actuator and sensor fault.

INDEX TERMS biped robot, fault-tolerant control, heterogeneous multi-agent system, robust H_{∞} control, S&R, smoothing signal model, UAV, hybrid UAVs-UGVs team system

I. INTRODUCTION

In recent years, the unmanned vehicle (UV) has attracted attention due to the advances in communication technology, sensing devices, and computing power. It not only reduces labor costs and brings convenience to life, but more importantly, it can replace some dangerous jobs for humans. Due to these benefits, it has been widely used in many scenarios, such as S&R, battlefield, logistics and transportation, surveillance, etc [1]. Compared with a single UV, multiple UVs can perform more complex tasks and are more robust due to a large number of agents [2]. However, the cost is that the design of such a multi-agent system (MAS) becomes more intricate as there are more problems to be resolved, such as formation, collision avoidance between agents, task allocation, and cooperation between agents [3]. In addition to the number increasment, a heterogeneous multi-agent system (HMAS) combining various types of UV is also valued

[4]. Compared with homogeneous multi-agent system, it can adapt to a wider variety of application scenarios because each agent has different aptitudes.

To construct an unmanned HMAS, the three required key capabilities are perception, decision-making and control. Perception is to obtain information through the sensor (e.g., localization or computer vision), decision-making is to make decisions through the sensor information, and control is to execute the decision through the actuator. To limit the scope of this paper, we focus on decision-making and control problem only. Three main problems of decision-making in an unmanned HMAS are task allocation, path planning and collision avoidance. Task allocation is to optimally assign tasks to each agent under some constraints such as agent capabilities, fuel cost, time cost, etc [5]. Path planning is to optimally plan paths for each agent while subject to constraints such as agent kinodynamic properties, distance,

obstacles collision, etc [6]. Collision avoidance is to avoid collision with obstacles. Although collision avoidance is often concerned in path planning, the collision avoidance system is also independently studied because of the requirements for the safety and reliability of the actual system [7].

Although there are many types of UVs to make up an unmanned HMAS, Unmanned Aerial Vehicle (UAV) and Unmanned Ground Vehicle (UGV) have been the subject of major recent research because of their availability and applicability. Additionally, the complementarity between them also makes such a system more potential [8]. In other words, UAV is widely used in reconnaissance due to the high mobility. However, the carrying capacity of UAV is very low compared to UGV since there is no ground support. In contrast, UGV has higher carrying capacity but is easily restricted by ground obstacles and cannot move at high speed. For these reasons, a hybrid UAVs-UGVs team system will be more appealing. To discuss more concretely, we consider a hybrid UAVs-UGVs team system for S&R. For the need for search mobility, we choose quadrotor aircraft as UAV. In order to deal with the complex terrain of the S&R environment, we choose biped robot as UGV. Even though other types of UGVs like wheeled robots and vehicles are easier to handle than biped robot, the high degree of freedom and the compatibility of the human environment still makes it a good candidate of UGV in a S&R system.

To the best of the authors' knowledge, most of the literature focus on only one specific problem in such an unmanned multi-agent S&R system, such as task allocation problem, path planning problem or control problem. Additionally, few literatures illustrate the relationship between these problems. This leads us to propose a system architecture of hybrid UAVs and biped robots team system (URTS) for S&R usage. The flowchart of decision-making and control process of URTS is also given. We divide it into five main hierarchical processes, i.e., task allocation, path planning, behavior layer, local motion planning and tracking control. It is because the UTRS needs to be able to assign different tasks to agents to perform first. After a task is assigned, if the task is to reach a goal location, a path to reach it needs to be planned. To make agent move on the path, a behavior corresponding to the environment is required to determine. Then, a local motion corresponding to the behavior of the agent needs to be designed. Finally, a controller must be designed to track the trajectory of the motion. In order to further limit the scope of the study, we will focus on the latter two processes. But to illustrate how the whole system works, the first three problems are also briefly stated.

The local motion planning is the bridge between path planning and tracking control since the path found by path planning algorithm and the path enforced to follow by a controller are not necessarily the same. The reason is that path planning algorithm usually treats the agent as a point, while the actual agent in the physical world is a mechanical system for the tracking control design. A mechanical system means that there exist kinodynamic constraints. This makes

certain paths impossible to follow for an actual agent, such as paths that are not smooth, have too large curvature, or require too large velocity and acceleration. Although some literatures directly tackle the kinodynamic constraints path planning problem [9], this paper splits path planning into three steps, i.e., (i) path planning, (ii) behavior layer and (iii) local motion planning for clarity. Through this decomposition, we can focus on the local motion planning of specific behaviors. The local motion planning of flying behavior for UAV and walking behavior for robot is studied in this paper, especially the latter. The local motion planning of biped robot walking, i.e., stable walking pattern generation, is a popular research topic due to its challenge [10].

The tracking control is to control an agent to follow a desired trajectory. There are many control strategies for MAS. According to the way of the design of controller, it can be divided into centralized control and decentralized control in control field [11]. Centralized control means there exists a powerful central controller in MAS to gather the state information of MAS and send the control command back to each agent to reach a global goal. Due to the powerful nature of the central controller, control commands can be determined well and quickly. But when it fails, the whole system will be completely paralyzed. In contrast, decentralized control means that each agent has its own controller to collect and control the agent's own state information. Under this architecture, although the global goal cannot be achieved, the possibility of paralyzing the entire system due to the failure of the controller can be avoided.

Besides, the formation control is also a topic in MAS [12]. Its purpose is to keep a MAS in a formation while moving. Although formation control provides a simple framework for the control of a large number of agents, considering the complexity of the disaster relief environment, formation will make the application of URTS inflexible. It is because we expect that agents in URTS need to organize multiple teams of different scales and types to deal with multiple tasks of different scales and types in a disaster relief environment. In this situation, it is more reasonable to treat each agent as an independent individual and specify an independent trajectory for each agent to follow.

In order to cope with the fault in the actual system, the fault-tolerant control (FTC) has also been widely studied. According to the way of handling the fault, it can be divided into the passive FTC and the active FTC [13]. The passive FTC treats the fault as an unknown system perturbation and designs a control law to tolerate it. In contrast, the active FTC will first estimate and identify the fault and then compensate it through the controller. Despite the added complexity in controller design, the active FTC will outperform the passive FTC due to the extra estimation steps. Based on the foregoing, a robust H_∞ decentralized observer-based feedforward-linearized PID FTC is proposed to deal with the control problem in URTS.

The contributions of this study are described as follows:

- 1) A system architecture and system flow of URTS for

the purpose of S&R are proposed so that the issues involved in URTS and their relationships can be defined and resolved.

- 2) A transformation between the trajectory generated by the path planning algorithm and the trajectory required for tracking control design is proposed to enable some common path planning algorithms can be applied to the tracking control of agents in URTS.
- 3) A general agent model is proposed so that the robust H_∞ decentralized observer-based tracking control problems of the heterogeneous agents in URTS, UAVs and biped robots, can be solved together.

The remainder of the paper is organized as follows. In Section II, a system architecture of URTS in S&R usage is proposed and the function and relationship of its components, i.e., task allocation, path planning, behavior layer, local motion planning and tracking control are described. In Section III, the system model of agents in URTS are given to design the motion of UAV flying and biped robot walking behavior and the control strategy of agents. In Section IV, a robust H_∞ decentralized observer-based feedforward-linearized PID FTC is proposed for the agents in URTS with the help of a general agent model. In Section V, a simulation example is given to illustrate the operation of the system architecture of URTS and to verify the effectiveness of the proposed tracking control method. In Section VI, a conclusion is made.

Notation 1: $\text{diag}(A_1, A_2, \dots, A_n)$: a block diagonal matrix with main diagonal blocks A_1, A_2, \dots, A_n . A^T : transpose of A . $A > 0$: a positive definite matrix. (a_n) : a sequence. (a_{k_n}) : a subsequence of a sequence (a_n) . $[a_{j,k}]$: A matrix with the entries $a_{j,k}$ in the j th row and k th column. $|S|$: size of a set S . \otimes : Kronecker product. I_n : n-dimension identity matrix. $x(t) \in L_2[0, t_f]$ if $\int_0^{t_f} x^T(t)x(t)dt < \infty$. $\text{Sym}(A)$: sum of a matrix A and its transposed, i.e., $\text{Sym}(A) = A + A^T$.

II. PRELIMINARIES OF URTS IN S&R USAGE

The URTS will start with a given S&R area, and end with mission completed. The URTS is composed of N_T teams and a ground station. Each team contains N_A agents with 1 UAV and $N_A - 1$ robots. Hence, the j th agent in the i th team is denoted as $\alpha_{i,j}$, where $i = 1, 2, \dots, N_T$ and $j = 1, 2, \dots, N_A$. The UAVs are chosen as the first agents in each team, i.e., $\alpha_{i,1}$. Each agent has environmental sensing capability and load capability, while the ground station is responsible for computing and decision-making. Besides, there are communication channels between agents and ground station through wireless network.

To complete search tasks, each team is designed to be responsible for a small area of the overall S&R area, and each agent will be assigned an appropriate path to cover the area. To complete rescue tasks, whenever a goal (e.g., victims or disaster area) is found by the machine vision of nearby agent, the ground station will assign some agents to the location of goal.

If a task is to reach a location of certain goal, we need to find a collision-free path to reach it. Hence, each agent will also sense distance-related information about its surrounding and send it back to the ground station. The ground station will combine this information with the goal location assigned by task allocation algorithm and make a decision to avoid obstacles and other agents nearby.

We need to determine specific behavior to follow the path found by path planning algorithm according to the situation of the environment especially for agents with complex mechanical systems like robots. Since such a system has a high degree of freedom, there are many ways to follow the same path (e.g., a robot can walk or run to follow the same path). Furthermore, agents in URTS are not always following the path. Sometimes they need the behavior such as stop to look around, get supplies and put supplies. To meet these needs, a behavioral layer is necessary.

In order to make a behavior, we must design a corresponding motion by local motion planning. The motion is a prescribed reference trajectory for an actual mechanical system to follow. Finally, a tracking controller is designed for each agent to follow this desired reference trajectory.

The agents overall have the same system architecture in URTS except for some subprocess differences. Followed by the concept in [14], a system architecture for an agent employed for S&R is proposed as shown in Fig. 1. The Simultaneous Localization And Mapping (SLAM) block converts sensor information into the location of agents q_{start} and an occupancy map C . The visual object recognition block provides distance information and object information through the analysis of sensor information. The object information provides agent machine vision that enables it to determine an appropriate behavior (e.g., a robot can see an obstacle and decides to climb through it). The detailed functions of remaining 5 blocks, i.e., Task Allocation, Path Planning, Behavior Layer, Local Motion Planning and Tracking Control, will be explained in the following subsections.

A. TASK ALLOCATION

In the URTS, it can be expected that each agent $\alpha_{i,j}$ will be assigned several specific tasks, such as searching a specific area, or delivering supplies to disaster area, etc. However, the number of agents and tasks is more than one, and each agent has different capabilities (e.g., moving speed or load capacity) and status (e.g., their own position or the amount of supplies carried), and each task has different characteristics (e.g., urgency, position, amount of supplies needed). Therefore, the results of task allocation can be "good or bad", which leads us to find the optimal allocation. This problem is referred to a task allocation problem or multi-robot task allocation problem. A problem formulation and a mathematical model of problem can be found in [15]. Although many different formulations and models have been employed to solve the task allocation problem, the common goal is to find a set of agent-task pairs to achieve a specific cost function. In this paper, we assume that the tasks have been properly assigned

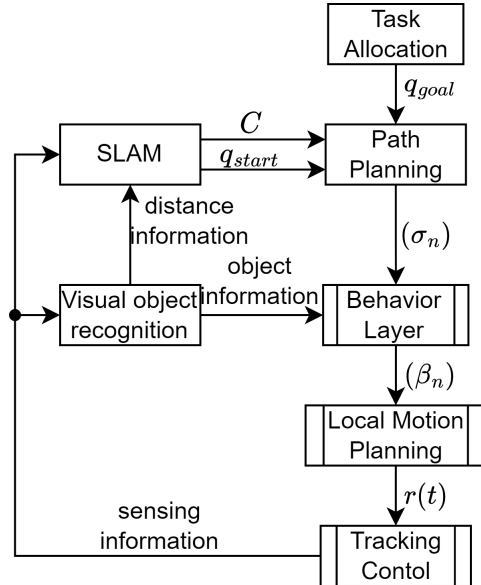


FIGURE 1: The system architecture of agent in URTS. The 2 blocks on left hand side are used to convert the low-level sensor information into high-level information, such as map, start point and object information. The 5 blocks on right hand side are the flow of an agent performing a S&R mission. From the top to the bottom, it is the decision of the task position, the planning of the path, the decision of the behavior, the planning of the local motion trajectory, and the low-level tracking control.

so that every agent knows a destination q_{goal} it needs to go at every moment.

Remark 1: This block is like a commander since it is used to assign task for agents. Thus, if the real S&R system has human experts as commanders, he can replace its job or make decisions together with it to maximize the rescue value.

Remark 2: Although each agent has its own team, agents can also work across teams. For example, if the result given by the task allocation algorithm contains the agent-task pairs $(\alpha_{1,5}, T_1)$ and $(\alpha_{2,2}, T_1)$, then the agent $\alpha_{1,5}$ in team 1 and the agent $\alpha_{2,2}$ in team 2 will execute task T_1 together.

B. PATH PLANNING

After a destination q_{goal} is assigned for each agent, next step is to find a collision-free path from current position to it. There must exist multiple feasible paths to go. Similar to task allocation, we usually want to find an optimal path. There are several path planning algorithm to handle this problem. Due to the developmental and universal nature of roadmap-based path planning algorithm, this paper considers it as the path planning method of UTRS. This method attempts to discretize the search space into interconnected roads and find the path on it.

According to the way of pathfinding, it can be divided into multi-query planner and single-query planner [16]. Multi-query planner will first construct a roadmap and then use

a graph search method on it to query the best path, such as Probability Road Map (PRM), Visibility Graph, and Voronoi Diagrams [17]. Single-query planner will complete the pathfinding by constructing and querying simultaneously, such as Rapidly-exploring Random Tree (RRT), Expansive Space Tree (EST), and Ariadne's Clew [16]. However, the environment is dynamic rather static for URTS so some extra structures need to impose on the aforementioned planner. Some common dynamic planners can also be found in [16], such as PRM with D* search algorithm, dynamic RRT, and extended RRT. All of the above common roadmap-based planners can be applied to the URTS.

Remark 3: To avoid agents colliding with each other, the concept of multi-agent path planning is proposed [18]. However, URTS operates in a large environment so the probability of collision is small and the agents have the ability to communicate. Therefore, when the paths collide, the mechanism of waiting for the other side to pass can be used to avoid the collision problem.

Furthermore, the constraints imposed by the mechanical structure are needed to consider within pathfinding process mentioned by other literatures but it will be left to local motion planning block to deal with. The reason is that URTS works on a complex environment and therefore requires a variety of behaviors to respond, and different behaviors have different constraints (e.g., curvature constraints between running and walking behavior are expected to be different for robot). In this case, a unified planner will become overly complex and impracticable. Therefore, we divide path planning into three subprocesses, i.e., path planning, behavior layer and local motion planning. The path planning block becomes a global planner and regard an agent as a point without kinodynamic constraints. The local motion planning block becomes a local planner and consider the motion planning of a specific behavior.

By treating a roadmap-based path planning algorithm as a black box, the output is a sequence (or sayed waypoints), and the three inputs are current configuration q_{start} , goal configuration q_{goal} , and configuration space C . Current configuration is obtained by GPS, inertial measurement unit, or other locating techniques. Goal configuration is obtained by the previous block, task allocation block. Configuration space C is constructed by environment information through sensors of agents online or in advance by human knowledge offline. C is a space containing all possible configurations of agents which are composed of free space C_{free} and obstacle space C_{obs} , where $C = C_{free} \cup C_{obs}$ and $C_{free} \cap C_{obs} = \emptyset$. For a simpler explanation of how the URTS works, the following assumptions are made.

Assumption 2.1: The locating ability of the URTS is perfect so every agent can know its current configuration q_{start} .

Assumption 2.2: A Task Allocation algorithm is already designed so that every agent can know its goal configuration q_{goal} .

Assumption 2.3: The URTS is supposed to have a perfect real-time mapping ability so a real-time configuration space

\mathcal{C} can be obtained.

Assumption 2.4: UAVs do not consider obstacle collision, so the path of UAVs can be directly assigned rather than found by planner. Robots do not consider obstacle collision in the direction perpendicular to the ground.

From above assumptions, a path of agent can be expressed as a sequence

$$(\sigma_n), n \in \mathbb{Z} \cap [1, k_f], \sigma_n \in \mathcal{C} \quad (1)$$

where k_f is the time step when reaching goal. Since the path planning is dynamic, (σ_n) is composed of multiple segments actually. Let (σ_{k_n}) be the subsequence of (σ_n) , where k_n is the time step when a replanning decision is occurred. Then, the segments of path from the result of the replanning in time step k_n can be expressed as sequences $(\sigma_m), m \in \mathbb{Z} \cap [k_n, k_{n+1}]$. For agents, the replanning decision can be due to a goal changing that is made by human or task allocation block. For robot, it can be a collision detected by a dynamic roadmap-based planner. The resulting path (σ_n) is passed to the next block, Behavior Layer.

C. BEHAVIOR LAYER

Path planning tells agents where to go but not how since we regard the agent as a point. Taking robot as an example, it may walk, run, climb, or jump to follow the path (σ_n) in real scenario. These behaviors with changing position are classified as "moving" behavior in this paper. Besides, the agents in the hybrid URTS do not always moving. Sometimes they have to suspend to take an action (e.g., getting and putting supplies, rotating in place to collect more environment information) or deal with some unexpected situations (e.g., no path found, the robot falls). These behaviors without changing position are classified as "action" behavior in this paper. More behaviors can be added so that the agent can have more ways to act with environment but there must have a corresponding behavior every moment otherwise the agent will lose control. The sequence of these behaviors can be expressed as:

$$(\beta_n), n \in \mathbb{Z} \cap [1, k_f], \beta_n \in \mathcal{B} \quad (2)$$

where \mathcal{B} is the set of behaviors. It is to say that the path (σ_n) is divided into many segments and each segment corresponds to a specific behavior. By the object information in Fig. 1, an appropriate behavior can be judged. However, it will be a rather complicated project, so this article only gives the structure of the behavior set. The behavior set \mathcal{B} of agent in URTS can be roughly described in Fig. 2.

D. LOCAL MOTION PLANNING

After a specific behavior is determined, the next step is to design a motion to achieve that behavior. Local motion planning block is like path planning block but its scale is smaller and its resolution and precision must be higher. Collision checking is needed since we consider agent as a point in path planning block and it is a real mechanical body

here. Furthermore, the kinodynamic constraint is handled in this block. Although motion planning and path planning are separated into two blocks, the technologies involved are similar and often with the same notion in other literature. Therefore, the output of this block is also a path but with a timescale, i.e., sampling period. This path is often referred as a desired reference trajectory $r(t)$. $r(t)$ describes the position and orientation that need to be reached over time by a machine system governed by a dynamic equation. Note that the path and trajectory are distinguished in some literature. Different from path (σ_n) , a trajectory $r(t)$ has considered the time in physic world. We also distinguish in this way in this article. The flowchart of local motion planning block is shown in Fig. 3

In Fig. 3, some basic behaviors of UAV and robot mentioned before are added to illustrate the flow of this block. To limit the scope of this article, we only focus on the motion planning of flying behavior of UAV and walking behavior of robot. They are belong to moving behavior in Fig. 3. A more detailed description will be given in the next section.

E. TRACKING CONTROL

If each agent in hybrid URTS can track each own reference trajectory $r(t)$, then they can move in the physical world as we expect. This is because the previous blocks have already completed all planning for the trajectory $r(t)$. All that remains is to track $r(t)$, to do so, a control method need to be design. It will be discussed detailly in Section IV. In addition, the sensing information collected by the sensors in this block is not only used for control but also sent back to the upper layer as shown in Fig. 1.

III. SYSTEM DESCRIPTION OF UAVS AND BIPED ROBOTS IN URTS

In order to design a reference trajectory $r(t)$ for the motion of UAV and robot, their dynamic models must be given first. After the system description of UAV and robot, the motion planning of flying and walking as shown in Fig. 4 will be discussed subsequently and separately in the next two subsections. Before the discussion of the motion planning of these two behaviors, the following assumption is made.

Assumption 3.1: The space between obstacles is large enough to eliminate the need for collision checking again, and the average speed of agents is slow enough to ignore dynamic constraints

However, for these two behaviors, there exists an inevitable kinematic constraint on the curvature of local motion. Although an accurate reference trajectory without breaking the curvature constraint can be designed, it is not easy to solve this problem. Additionally, it is not necessary for these two behaviors in URTS since they are used to move from one location to another while the effect of error during moving caused by breaking the curvature constraint is relatively insignificant. At the same time, the *Assumption 3.1* makes sure the error will not cause collision. As an alternative, this problem can be handled by curve fitting

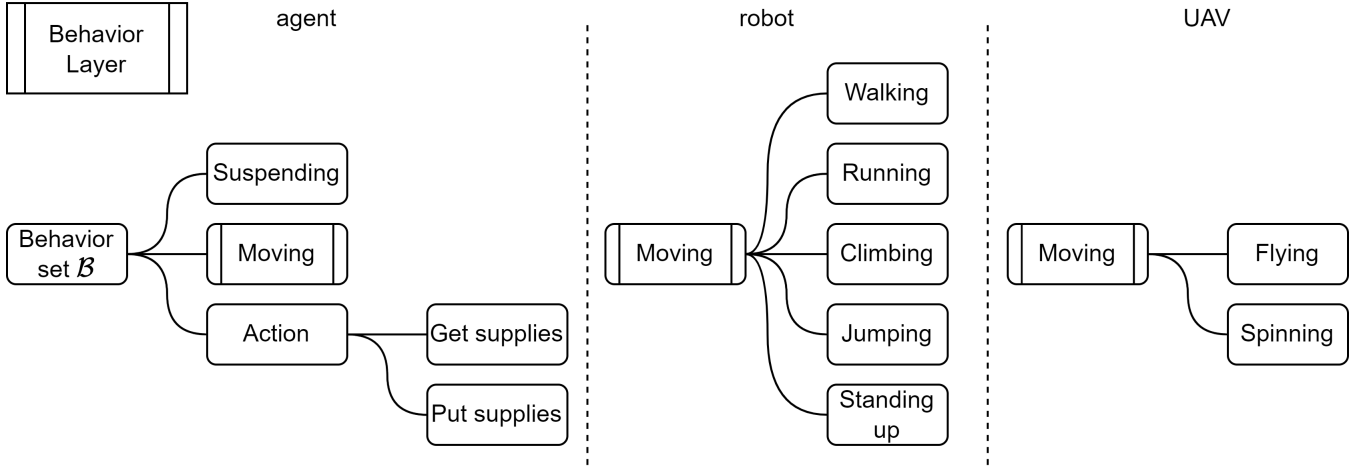


FIGURE 2: The structure of behavior layer. The leaves of the tree structure are the possible behaviors an agent can take. The behavior to be took at every moment will be decided in this block.

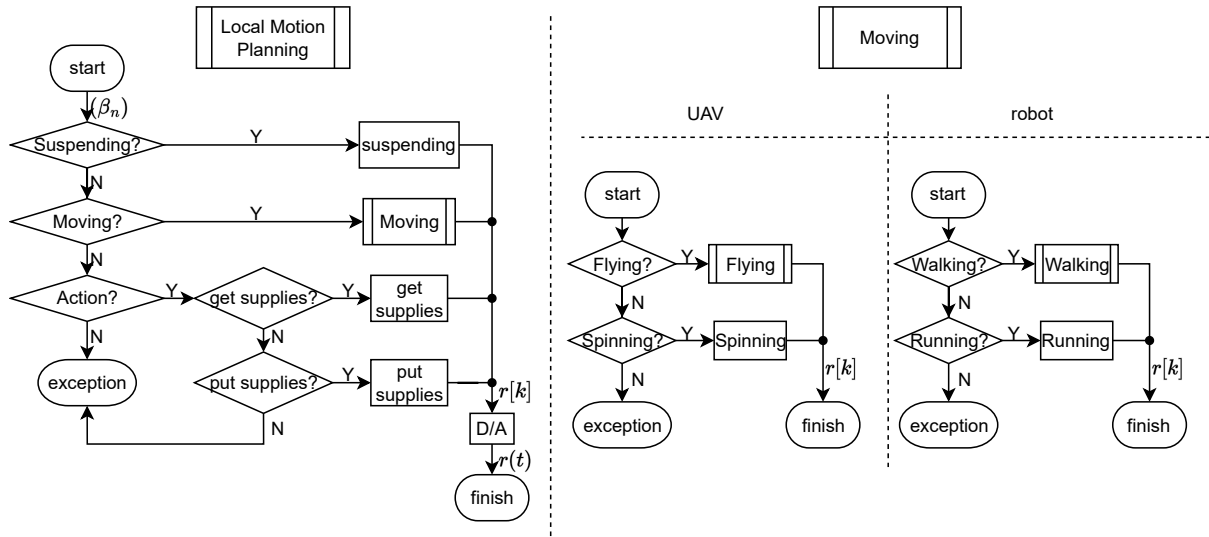


FIGURE 3: The flowchart of local motion planning. The corresponding motion planning will be executed according to the behavior determined by the behavior layer. The exception terminator in figure represents an exceptional condition that performs unconsidered behaviors. The reference path $r[k]$ is a sequence (or say a discrete signal) designed by a specific behavior block. $r[k]$ will be converted to the desired reference trajectory $r(t)$, an analog signal, by an A to D convertor.

which can be regarded as a post-process of the path (σ_n) . The post-process will appear in the beginning of motion planning process of these two behaviors as shown in Fig. 4.

A. MOTION PLANNING OF FLYING OF UAV

A dynamic model about how the UAV moves in the physical world is given first. By Newton-Euler equation, the dynamic model of UAV can be formulated as [19]:

$$\begin{bmatrix} F \\ \tau \end{bmatrix} = \begin{bmatrix} mI & 0 \\ 0 & J \end{bmatrix} \begin{bmatrix} \ddot{X} \\ \ddot{\Theta} \end{bmatrix} + \begin{bmatrix} 0 \\ \dot{\Theta} \times (J\dot{\Theta}) \end{bmatrix} + \begin{bmatrix} f_g \\ 0 \end{bmatrix} + \begin{bmatrix} K_F & 0 \\ 0 & K_\tau \end{bmatrix} \begin{bmatrix} \dot{X} \\ \dot{\Theta} \end{bmatrix} \quad (3)$$

$$\text{where } J = \begin{bmatrix} J_x & 0 & 0 \\ 0 & J_y & 0 \\ 0 & 0 & J_z \end{bmatrix}, \quad K_F = \begin{bmatrix} K_x & 0 & 0 \\ 0 & K_y & 0 \\ 0 & 0 & K_z \end{bmatrix},$$

$$K_\tau = \begin{bmatrix} K_{\tau_x} & 0 & 0 \\ 0 & K_{\tau_y} & 0 \\ 0 & 0 & K_{\tau_z} \end{bmatrix}, \quad F = \begin{bmatrix} f_x \\ f_y \\ f_z \end{bmatrix} = R(\Theta) \begin{bmatrix} 0 \\ 0 \\ F \end{bmatrix},$$

$$\tau = \begin{bmatrix} \tau_x \\ \tau_y \\ \tau_z \end{bmatrix}, \quad X = \begin{bmatrix} x \\ y \\ z \end{bmatrix}, \quad \Theta = \begin{bmatrix} \phi \\ \theta \\ \psi \end{bmatrix}, \quad f_g = \begin{bmatrix} 0 \\ 0 \\ -mg \end{bmatrix}, \quad R(\Theta) = R_z(\psi)R_y(\theta)R_x(\phi), \quad R_z(\psi) =$$

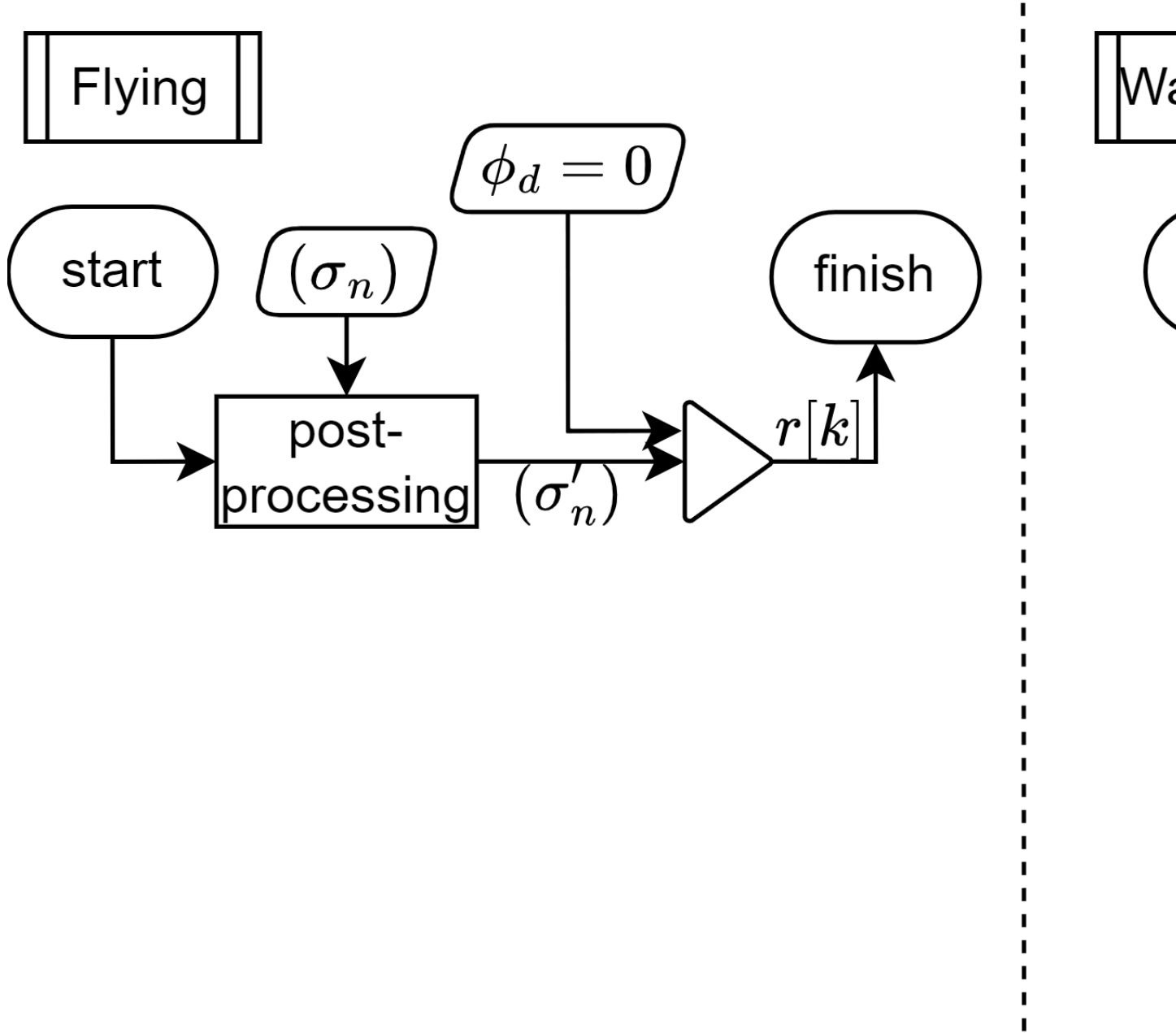


FIGURE 4: The flowchart of Flying and Walking. In both blocks, a smoothed path is obtained by post-processing first. Then the respective motion of behavior is designed. The final outputs of Flying and Walking are all desired reference path $r[k]$, but its value and dimension will vary according to the dimension of the system model.

$$\begin{aligned}
 & \begin{bmatrix} \cos \psi & -\sin \psi & 0 \\ \sin \psi & \cos \psi & 0 \\ 0 & 0 & 1 \end{bmatrix}, R_y(\theta) = \begin{bmatrix} \cos \theta & 0 & \sin \theta \\ 0 & 1 & 0 \\ -\sin \theta & 0 & \cos \theta \end{bmatrix}, \\
 & R_x(\phi) = \begin{bmatrix} 1 & 0 & 0 \\ 0 & \cos \phi & -\sin \phi \\ 0 & \sin \phi & \cos \phi \end{bmatrix}. g \text{ is the gravity acceleration, } m \text{ and } J \text{ are the mass and inertia matrix of UAV, respectively, } \tau \text{ and } F \text{ are the total torque and force acting on UAV, respectively, } \Theta \text{ is the Euler angles in body frame, } X \text{ is the position of center of mass (CoM) in inertial frame,}
 \end{aligned}$$

K_τ and K_F are the aerodynamic damping coefficients, and $R(\Theta)$ is the intrinsic rotation matrix from body frame to inertial frame. This model treats the UAV as a mass point and can control the force in the z direction and the torque in the x , y and z direction. Hence, the reference trajectory of UAV $r(t) = [x_r(t), y_r(t), z_r(t), \phi_r(t), \theta_r(t), \psi_r(t)]^T \in \mathbb{R}^6$, where the subscript r denotes the reference.

Now, suppose the UAV flying occurs between time step t_1 and t_2 , that is, $\beta_n = \text{flying}$, $n \in \mathbb{Z} \cap [t_1, t_2]$. The corresponding path (σ_n) , $n \in \mathbb{Z} \cap [t_1, t_2]$ will be smoothed

first by linear interpolation and then by cubic spline interpolation, which gives the smoothed path $(\sigma'_n), n \in \mathbb{Z} \cap [t_1, t_1 + D(t_2 - t_1)], \sigma'_n \in \mathbb{R}^3$, where $D \in \mathbb{Z}^+$ is the interpolation density. Then, (σ'_n) will be the position reference path $[x_r[k], y_r[k], z_r[k]]^T$. Subsequently, the orientation reference path, roll angle $\phi_r[k]$, pitch angle $\theta_r[k]$ and yaw angle $\psi_r[k]$ are all considered. $\phi_r[k]$ is set to zero since no need for spinning when flying. $\theta_r[k]$ and $\psi_r[k]$ cannot be set beforehand since UAV is an underactuated system, which will be discussed in the next section. Finally, the reference path $r[k]$ of UAV can be obtained by combining them together, i.e., $r[k] = [x_r[k], y_r[k], z_r[k], \psi_r[k]]^T$. The flowchart is shown in Fig. 4.

B. MOTION OF WALKING OF ROBOT

By Lagrange equation, the dynamic model of biped robot can be formulated as:

$$\tau = M(q)\ddot{q} + C(q, \dot{q})\dot{q} + G(q) \quad (4)$$

where $q, \dot{q}, \ddot{q} \in \mathbb{R}^{12}$ are angular position, angular velocity, and angular acceleration vector of revolute joints, $M(q) \in \mathbb{R}^{12 \times 12}$ is the inertia matrix, $C(q, \dot{q}) \in \mathbb{R}^{12}$ is the Coriolis and centripetal force vector and $G(q) \in \mathbb{R}^{12}$ is the gravitational force vector. The detailed kinematic and dynamic parameters can be found in the online source [20]. For robot, the reference trajectory $r(t) = q_r(t) \in \mathbb{R}^{12}$ is in the joint space. Furthermore, the walking of biped robot suffers from the falling problem, i.e., how to find a stable walking pattern to prevent robot from falling. These make the design of walking motion more difficult. In this paper, a three-dimensional linear inverted pendulum Model (3D-LIPM) [21] is used to design the walking motion.

With 3D-LIPM, we can significantly reduce the amount of computation. Let us define the body frame of robot as $\{\widehat{X}_b, \widehat{Y}_b, \widehat{Z}_b\}$ as in [20]. Taking the forward direction of robot as \widehat{X}_b direction, the left direction as \widehat{Y}_b direction, and the torso direction as \widehat{Z}_b direction in body frame, "Falling" means the moments on the robot in \widehat{X}_b and \widehat{Y}_b direction are not zero. More accurately, the robot will not fall if the zero moment point (ZMP) lies in the support polygon, i.e., the convex hull of face of supported foots. The ZMP in \widehat{X}_b direction can be described as [22] (The ZMP in \widehat{Y}_b direction as the same form):

$$x_{zmp} = \frac{\sum_{i=1}^{12} (m_i(\ddot{z}_i + g)x_i - m_i\ddot{x}_i z_i - I_{iy}\ddot{\Omega}_{iy})}{\sum_{i=1}^{12} m_i(\ddot{z}_i + g)} \quad (5)$$

where m_i is the CoM, x_i, z_i are the linear position components, I_{iy} is the inertial component, and $\ddot{\Omega}_{iy}$ is the angular velocity component of link i . However, it is difficult to directly calculate the analytical solution of q_r through (6). Since there is a complex coordinate transformation between q_r and $x_i, z_i, \ddot{\Omega}_{iy}$. At the same time, it is necessary to ensure that x_{zmp} falls on the support polygon but the support polygon also has a relationship with q_r . To simplify this complex

problem, an approximate solution can be derived through 3D-LIPM. It is to find CoM reference first and then obtain $q_r(t)$ by using inverse kinematic (IK) with given step size, step height, step period and CoM height. Many researchers have used this method to avoid complex calculations for ZMP of actual robot dynamic model. Although there exist a model error between the actual dynamic model and 3D-LIPM, the design process will be more simple. The overall process is shown in Fig. 4.

Following the same step in UAV, the smoothed path (σ'_n) for robot can be obtained at first. For the convenience of explanation, suppose walking is occurred between time step 1 and N , i.e., $n \in \mathbb{Z} \cap [1, N]$. Note that (σ'_n) is not actual CoM reference in robot case since CoM of robot need to "swinging" for balance. Despite that, (σ'_n) tells the robot the position to go so the \widehat{X}_b direction can be obtained by doing finite difference on (σ'_n) due to the expectation that the robot will move forward (rather than sideways or backward). To keep torso upright, the \widehat{Z}_b direction is equal to the z -axis in the inertial frame \widehat{Z}_g . Given \widehat{X}_b and \widehat{Z}_b , \widehat{Y}_b can be obtained obviously through cross product. The sequence of body frame, i.e., CoM orientation path (CO_n) can be obtained through the above steps.

Remark 4: A frame in \mathbb{R}^3 can be determined by giving the "position" and "orientation" with respect to a reference frame. That is, given the position and orientation of two joints in a link with known kinematics, the position and orientation of joints between them can be found by IK. Hence, we need to find the position path and orientation path, which compose the desired path.

Let us denote the x and y component of σ'_n in (σ'_n) as the sequence $(\sigma_n^1), \sigma_n^1 \in \mathbb{R}^2$. The left and right "envelopes", (σ_n^2) and (σ_n^3) , of (σ_n^1) with a fixed distance L_1 can be found by (σ_n^1) and (CO_n) through the geometric relation between $(\sigma_n^i), i = 1, 2, 3$, where L_1 is feet width (or shoulder width). Then the x and y component of left and right foothold paths, $(\sigma_{k_n}^2)$ and $(\sigma_{k_n}^3)$, can be obtained by a given step size, which are the subsequence of (σ_n^2) and (σ_n^3) , respectively. Finally, left and right foothold paths $(\sigma_{k_n}^i), \sigma_{k_n}^i \in \mathbb{R}^3, i = 4, 5$ are found by adding z component which is given by ground height.

After foothold paths are obtained, ankle position path can also be obtained by the given step height which is customized by the designer or based on the height of the obstacle to be crossed. Taking the left foothold path as an example, x and y component of the highest position of ankle during stride are set as middle point of two footholds $\sigma_{k_m}^2$ and $\sigma_{k_{m+1}}^2$ where $m \in \mathbb{Z} \cap [1, N - 1]$, and the z component is given by step height. By using cubic spline interpolation, we have the left and right ankle position paths, (σ_n^6) and (σ_n^7) . The ankle orientation path is found by the gradient of ground. Finally, the left and right ankle paths, (σ_n^8) and (σ_n^9) , are found by combining the position and orientation path together. So far, the remaining work is to find out the CoM path and then to combine with the ankle path to calculate the joint path through IK.

To obtain CoM position path (CP_n), ZMP path needs to be obtained first. ZMP path can be obtained through foothold paths ($\sigma_{k_n}^4$) and ($\sigma_{k_n}^5$) since ZMP needs to lie in the support face and the foothold path points out when the feet are on the ground. Suppose the CoM height z_c of robot is constant when walking, then the robot model can be regarded as an 3D-LIPM:

$$\begin{aligned}\ddot{x}_c &= \frac{g}{z_c}(x_c - p_x) \\ \ddot{y}_c &= \frac{g}{z_c}(y_c - p_y)\end{aligned}\quad (6)$$

where (x_c, y_c, z_c) is the position of CoM of the inverted pendulum, g is the gravity acceleration, and (p_x, p_y) is the position of ZMP on the x - y plane. Since z_c , g and (p_x, p_y) are given, (x_c, y_c) can be solved. Observing the dynamic equations in the x and y directions in (6), it can be found that they are decoupled and thus can be calculated separately. Therefore, only the solution in the x direction is given below (the y direction as the same). To solve it, a method is proposed to convert it to a servo problem [23]:

$$\begin{aligned}\dot{\bar{x}}_c &= A\bar{x}_c + Bu \\ p_x &= C\bar{x}_c\end{aligned}\quad (7)$$

where $\bar{x}_c = \begin{bmatrix} x_c \\ \dot{x}_c \\ \ddot{x}_c \end{bmatrix}$, $A = \begin{bmatrix} 0 & 1 & 0 \\ 0 & 0 & 1 \\ 0 & 0 & 0 \end{bmatrix}$, $B = \begin{bmatrix} 0 \\ 0 \\ 1 \end{bmatrix}$, and $C = [1 \ 0 \ -z_c/g]$. Our goal is to find a control input u in order that the output p_x can track a ZMP reference trajectory so that the solution x_c of ODE in (6) can be obtained, i.e., the CoM position path is found. Unlike conventional methods, the problem is solved by the optimal control. The system is discretized first and the discrete LQ tracker is employed to achieve the output tracking. The formulation can be found in TABLE 4.4-1 in [24]. The CoM position path (CP_n) then be obtained by combining x_c and y_c with z_c .

By combining the CoM orientation path (CO_n) and position path (CP_n), CoM path can be obtained. Finally, the joint path, i.e., reference path $r[k]$ of robot can be found by solving IK.

IV. REFERENCE TRACKING CONTROL

After the reference trajectory $r(t)$ is set, the last step is to design a controller for an agent to track it. To analyze the tracking control problem of UAV model in (3) and robot model in (4) together, we represent them by the same form called agent model through some appropriate variable transformations:

$$M(x(t))\ddot{x}(t) + H(x(t), \dot{x}(t)) = u(t) \quad (8)$$

where $u(t) \in \mathbb{R}^n$ is control input vector, $x(t) \in \mathbb{R}^n$ is state vector, $M(\cdot) \in \mathbb{R}^{n \times n}$ is inertia matrix, and $H(\cdot, \cdot) \in \mathbb{R}^n$ is non-inertial force vector. The control law is given as:

$$u(t) = M(r(t))(\ddot{r}(t) + u_{fb}(t)) + H(r(t), \dot{r}(t)) \quad (9)$$

where $M(r(t)), \ddot{r}(t), H(r(t), \dot{r}(t))$ are the feedforward control terms for canceling system nonlinearity, and $u_{fb}(t)$ is the feedback control law for improving system robustness.

To make the model more realistic, the following external disturbances encountered in actual scenarios are considered:

- 1) For agent, there exists coupling effect due to co-channel interference in communication between agents [25].
- 2) For agent, there exists cyber-attack on communication network between agents and ground station.
- 3) For agent, there exists sensor noise.
- 4) For UAV, there exists wind disturbance [26].
- 5) For robot, there exists ground reaction force [27].

Let $x_{i,j}(t), i = 1, 2, \dots, N_T, j = 1, 2, \dots, N_A$ denote the state vector of agents $\alpha_{i,j}$. The coupling term can be represented as

$$\sum_{k=1, k \neq i}^{N_T} h_{i,1,k}(x_{i,1}(t))x_{k,1}(t) \quad (10)$$

for UAVs $\alpha_{i,1}$ and

$$\sum_{k=1, k \neq j'}^{N_A} h_{i,j',k}(x_{i,j'}(t))x_{i,k}(t) \quad (11)$$

for robots $\alpha_{i,j'}$ where $j' = 2, 3, \dots, N_A$ [25]. Since the ground station is responsible for the calculation, the calculated control command (9) will be transmitted to the agent through the network channel in URTS. Therefore, the coupling effect due to co-channel interference and the cyber-attack signal will deteriorate the control command. In addition, the wind disturbance and the ground reaction force will apply extra force on an agent (8). Therefore, through appropriate conversion, the above disturbances can be equivalent to a disturbance force $d_1(t)$. The nominal system (8) then be rewritten as the following real system:

$$M(x(t))\ddot{x}(t) + H(x(t), \dot{x}(t)) = u(t) + d_1(t) \quad (12)$$

Now, substituting (9) into (12) and subtracting $M(x(t))\ddot{r}(t)$ from the left and right sides, we have:

$$\begin{aligned}M(x(t))(\ddot{x}(t) - \ddot{r}(t)) + H(x(t), \dot{x}(t)) \\ = (M(r(t)) - M(x(t)))\ddot{r}(t) + M(r(t))u_{fb}(t) \\ + H(r(t), \dot{r}(t)) + d_1(t)\end{aligned}\quad (13)$$

By Multipling $M(x(t))^{-1}$ from the left and right sides and with some arrangments, we have:

$$\ddot{e}(t) = u_{fb}(t) + f_1(t) \quad (14)$$

where $f_1(t) = M(x(t))^{-1}(-\Delta M(\ddot{r}(t) + u_{fb}(t)) - \Delta H + d_1(t)) \in \mathbb{R}^n$ is the actuator fault signal, $\Delta M \triangleq M(x(t)) - M(r(t))$, $\Delta H \triangleq H(x(t), \dot{x}(t)) - H(r(t), \dot{r}(t))$ are the error terms from feedforward compensation, and $e(t) = x(t) - r(t)$ is the tracking error. Let $e(t) = \left[\int_0^t e^T(\tau)d\tau \ e^T(t) \ \dot{e}^T(t) \right]^T \in \mathbb{R}^{3n}$ be the PID tracking error, (14) can be rewrited as:

$$\dot{e}(t) = Ae(t) + B(u_{fb}(t) + f_1(t)) \quad (15)$$

where $A = A_0 \otimes I_n, B = B_0 \otimes I_n$ with $A_0 = \begin{bmatrix} 0 & 1 & 0 \\ 0 & 0 & 1 \\ 0 & 0 & 0 \end{bmatrix}, B_0 = \begin{bmatrix} 0 \\ 0 \\ 1 \end{bmatrix}$.

Through above analysis, the tracking control problem of the nonlinear system with external disturbance (12) is transformed into the stable control problem of the linear system (15) with fault signal by the feedforward linearization. The remaining step is to design an appropriate feedback control law $u_{fb}(t)$ to make the linear system stable. In a real system, the feedback information is measured by sensor, i.e., the state $x(t)$ in (8) is unavailable. At the same time, the external disturbances on sensor also need to be considered as mentioned before. Since the sensor information will transmitted back to the ground station for calculating control command through the network channel in URTS, not only the sensor noise but also the coupling effect due to co-channel interference and the cyber-attack signal are concerned. Let $\mathbf{x}(t) = \left[\int_0^t x^T(\tau)d\tau \quad x^T(t) \quad \dot{x}^T(t) \right]^T$, the measurement output equation can be described as:

$$y(t) = C\mathbf{x}(t) + B_2 f_2(t) \quad (16)$$

where $y(t) \in \mathbb{R}^l$ is the output vector, $C \in \mathbb{R}^{l \times 3n}$ is the output matrix, $B_2 \in \mathbb{R}^{l \times o}$ is the input matrix of $f_2(t)$, and $f_2(t) \in \mathbb{R}^o$ is the actuator fault signal. Let $\mathbf{r}(t) = \left[\int_0^t r^T(\tau)d\tau \quad r^T(t) \quad \dot{r}^T(t) \right]^T$ to modify the output equation (16) and putting it and (15) together, we have the following system:

$$\begin{aligned} \dot{\mathbf{e}}(t) &= A\mathbf{e}(t) + B(u_{fb}(t) + f_1(t)) \\ y(t) &= C\mathbf{e}(t) + Cr(t) + B_2 f_2(t) \end{aligned} \quad (17)$$

To deal with the fault signals $f_i(t), i = 1, 2$, a smoothing signal model is introduced [28]:

$$\begin{aligned} \dot{F}_i(t) &= A_i F_i(t) + v_i(t) \\ f_i(t) &= C_i F_i(t) \end{aligned} \quad (18)$$

where $F_i(t) = [f_i^T(t) \quad f_i^T(t-h) \quad \dots \quad f_i^T(t-kh)]^T \in \mathbb{R}^{(k+1)n}, A_i \in \mathbb{R}^{(k+1)n \times (k+1)n}, v_i(t)$ is the model error, $C_i = [1 \quad 0 \quad \dots \quad 0] \otimes I_{n_i}$, and k is the smoothing signal model window size with $n_1 = n$ and $n_2 = o$. Substituting (18) into (17), we get:

$$\begin{aligned} \dot{\bar{e}}(t) &= \bar{A}\bar{e}(t) + \bar{B}u_{fb}(t) + \bar{v}(t) \\ y(t) &= \bar{C}\bar{e}(t) + Cr(t) \end{aligned} \quad (19)$$

where $\bar{e}(t) = \begin{bmatrix} \mathbf{e}(t) \\ F_1(t) \\ F_2(t) \end{bmatrix}, \bar{A} = \begin{bmatrix} A & BC_1 & 0 \\ 0 & A_1 & 0 \\ 0 & 0 & A_2 \end{bmatrix}, \bar{B} = \begin{bmatrix} B \\ 0 \\ 0 \end{bmatrix}$,

$\bar{C} = [C \quad 0 \quad B_2 C_2]$, and $\bar{v}(t) = \begin{bmatrix} v_1(t) \\ v_2(t) \end{bmatrix}$. Since the fault signals become a state variable of the augment system in (19), a Luenberger observer is proposed to estimate them and origin state simultaneously to achieve active FTC:

$$\begin{aligned} \dot{\hat{e}}(t) &= \bar{A}\hat{e}(t) + \bar{B}u_{fb}(t) - L(y(t) - \hat{y}(t)) \\ \hat{y}(t) &= \bar{C}\hat{e}(t) + Cr(t) \end{aligned} \quad (20)$$

Assumption 4.1: The augmented system (19) is observable. The PID FTC law is given as:

$$u_{fb}(t) = K\hat{e}(t) \quad (21)$$

where $K = [K_I \quad K_P \quad K_D \quad K_{F_1} \quad K_{F_2}]$ is the total control gain, K_P, K_I, K_D are the PID control gain for position tracking error $e(t)$, and $K_{F_i}, i = 1, 2$ are the fault control gain. Let us define the estimation error $\tilde{e}(t) = \bar{e}(t) - \hat{e}(t)$, by the two subsystems (19) and (20), we get:

$$\dot{\tilde{e}}(t) = \bar{A}\tilde{e}(t) + L\bar{C}\tilde{e}(t) \quad (22)$$

Combining (19), (21), and (22), we have the following augmented system:

$$\dot{\tilde{x}}(t) = \tilde{A}\tilde{x}(t) + \tilde{v}(t) \quad (23)$$

where $\tilde{x}(t) = \begin{bmatrix} \bar{e}(t) \\ \tilde{e}(t) \end{bmatrix}, \tilde{A} = \begin{bmatrix} \bar{A} + \bar{B}K & -\bar{B}K \\ 0 & \bar{A} + \bar{C}L \end{bmatrix}$, and $\tilde{v}(t) = \begin{bmatrix} \bar{v}(t) \\ \tilde{v}(t) \end{bmatrix}$

In order to enable the designed control gain K and observer gain L to achieve a specific stabilized performance for the system (23) under the disturbance $\bar{v}(t)$, the H_∞ observer-based stabilized control performance below a prescribed disturbance attenuation level ρ^2 is given as:

$$\frac{\int_0^{t_f} (\tilde{x}^T(t)Q\tilde{x}(t) + u_{fb}^T(t)Ru_{fb}(t))dt - V(\tilde{x}(0))}{\int_0^{t_f} \tilde{v}^T(t)\tilde{v}(t)dt} \leq \rho^2 \quad (24)$$

where t_f is the final time, $Q \geq 0$ is the weighting matrix of augmented state, $R > 0$ is the weighting matrix of control effort, $V(\tilde{x}(0))$ is the initial condition effect on augmented system (23), and $\tilde{v}(t)$ is the total disturbance needs to be attenuated. If we can find the control gain K and observer gain L such that (24) holds, then the effect of total disturbance $\tilde{v}(t)$ on augmented state $\tilde{x}(t)$ can be attenuated to a prescribed level ρ^2 from the viewpoint of energy. Before analyzing the H_∞ observer-based stabilized control problem in (24), the following lemmas are given:

Lemma 1 ([29]): For any matrices X and Y with appropriate dimensions, and matrix $R = R^T > 0$ the following inequality holds:

$$X^T Y + Y^T X \leq X^T R^{-1} X + Y^T R Y \quad (25)$$

Lemma 2 (Schur Complement [29]): For the matrices $X = X^T, Y = Y^T$ and matrix R with appropriate dimensions the following statement is true:

$$\begin{bmatrix} X & R \\ R^T & Y \end{bmatrix} > 0 \Leftrightarrow Y > 0, X - RY^{-1}R^T > 0 \quad (26)$$

Then, the following theorem is given.

Theorem 1: If there exists matrices $P = P^T > 0, K, L$ such that the following matrix inequality hold:

$$Q + P\tilde{A} + \tilde{A}^T P + \tilde{K}^T R\tilde{K} + \frac{1}{\rho^2} PP \leq 0 \quad (27)$$

where $\tilde{K} = [K \quad -K]$, then the H_∞ observer-based stabilized control specification (24) can be achieved.

Proof. Choose the Lyapunov function $V(\tilde{x}(t)) = \tilde{x}^T(t)P\tilde{x}(t)$ for the augmented system (23) with $P = P^T > 0$, we have:

$$\begin{aligned} & \int_0^{t_f} (\tilde{x}^T(t)Q\tilde{x}(t) + u_{fb}^T(t)Ru_{fb}(t))dt \\ &= V(\tilde{x}(0)) - V(\tilde{x}(t_f)) + \int_0^{t_f} (\tilde{x}^T(t)Q\tilde{x}(t) \\ &+ u_{fb}^T(t)Ru_{fb}(t) + \dot{V}(\tilde{x}(t)))dt \\ &\leq V(\tilde{x}(0)) + \int_0^{t_f} (\tilde{x}^T(t)Q\tilde{x}(t) + \\ &u_{fb}^T(t)Ru_{fb}(t) + Sym(\dot{\tilde{x}}^T(t)P\tilde{x}(t)))dt \end{aligned} \quad (28)$$

By (23) and Lemma 1, we have:

$$\begin{aligned} & Sym(\dot{\tilde{x}}^T(t)P\tilde{x}(t)) \\ &= Sym((\tilde{A}\tilde{x}(t) + \tilde{v}(t))^T P\tilde{x}(t)) \\ &= \tilde{x}^T(t)(P\tilde{A} + \tilde{A}^T P + \frac{1}{\rho^2}PP)\tilde{x}(t) + \rho^2\tilde{v}^T(t)\tilde{v}(t) \end{aligned} \quad (29)$$

Substituting (29) and (21) into (28), we get:

$$\begin{aligned} & \int_0^{t_f} (\tilde{x}^T(t)Q\tilde{x}(t)dt + u_{fb}^T(t)Ru_{fb}(t))dt \\ &\leq V(\tilde{x}(0)) + \int_0^{t_f} (\tilde{x}^T(t)(Q + P\tilde{A} + \tilde{A}^T P + \tilde{K}^T R\tilde{K} \\ &+ \frac{1}{\rho^2}PP)\tilde{x}(t) + \rho^2\tilde{v}^T(t)\tilde{v}(t))dt \end{aligned}$$

Thus, if (27) holds then (24) holds ■

Although the sufficient condition (27) for the existence of the H_∞ observer-based stabilized control specification (24) have been found, it can not be solved easily since it is a bilinear matrix inequality (BMI) and exists strong coupling between the variables. To solve the issue, a two-step design is exploit.

Step 1: First, let the Lyapunov function of augmented system (23) be the sum of two Lyapunov function of subsystems (19) and (22), i.e., $V(\tilde{x}(t)) = \tilde{x}^T(t)P\tilde{x}(t) = \bar{e}^T(t)P_1\bar{e}(t) + \tilde{e}^T(t)P_2\tilde{e}(t)$. Second, let the augmented state energy be the sum of tracking error energy and estimated error energy, i.e., $\tilde{x}^T(t)Q\tilde{x}(t) = \bar{e}^T(t)Q_1\bar{e}(t) + \tilde{e}^T(t)Q_2\tilde{e}(t)$. Substituting $P = \begin{bmatrix} P_1 & 0 \\ 0 & P_2 \end{bmatrix}$ and $Q = \begin{bmatrix} Q_1 & 0 \\ 0 & Q_2 \end{bmatrix}$ into (27), we get:

$$\begin{aligned} & \begin{bmatrix} Q_1 & 0 \\ 0 & Q_2 \end{bmatrix} + Sym\left(\begin{bmatrix} P_1 & 0 \\ 0 & P_2 \end{bmatrix}\right) \begin{bmatrix} \bar{A} + \bar{B}K & -\bar{B}K \\ 0 & \bar{A} + L\bar{C} \end{bmatrix} \\ &+ \begin{bmatrix} K^T R K & -K^T R K \\ -K^T R K & K^T R K \end{bmatrix} + \frac{1}{\rho^2} \begin{bmatrix} P_1 P_1 & 0 \\ 0 & P_2 P_2 \end{bmatrix} \\ &= \begin{bmatrix} M_{11} & -P_1 \bar{B}K - K^T R K \\ * & M_{22} \end{bmatrix} < 0 \end{aligned} \quad (30)$$

where $M_{11} = Q_1 + Sym(P_1(\bar{A} + \bar{B}K)) + K^T R K + \frac{1}{\rho^2}P_1 P_1$, $M_{22} = Q_2 + Sym(P_2(\bar{A} + L\bar{C})) + K^T R K + \frac{1}{\rho^2}P_2 P_2$. By the fact that $\begin{bmatrix} M_{11} & -P_1 \bar{B}K - K^T R K \\ * & M_{22} \end{bmatrix} < 0 \Rightarrow M_{11} < 0, M_{22} < 0$, the inequality $M_{11} < 0$ is used to find P_1, K .

Premultiplying and postmultiplying $M_{11} < 0$ by $W_1 = P_1^{-1}$ and applying Lemma 2, we obtain:

$$\begin{bmatrix} Sym(\bar{A}W_1 + \bar{B}Y_1) + \frac{1}{\rho^2} & W_1^{-1/2}\sqrt{Q_1} & Y_1^T \\ * & -I & 0 \\ * & * & -R^{-1} \end{bmatrix} < 0 \quad (31)$$

where $Y_1 = KW_1$. By solving the LMI (31), we can obtain W_1, Y_1 .

Step 2: Substituting $P_1 = W_1^{-1}$ and $K = Y_1 W_1^{-1}$ found in *Step 1* into (30) and applying Lemma 2, we obtain:

$$\begin{bmatrix} M_{11} & -P_1 \bar{B}K - K^T R K & P_2 \\ * & Q_2 + Sym(P_2 \bar{A} + Y_2 \bar{C}) + K^T R K & 0 \\ * & * & -\rho^2 I \end{bmatrix} < 0 \quad (32)$$

where $Y_2 = P_2 L$. By solving the LMI (32), we can obtain P_2, Y_2 .

If we want to find the optimal H_∞ observer-based stabilized control specification for the system (23), we need to solve the following LMIs-constrained optimization problem:

$$\begin{aligned} \rho^* &= \min_{P, K, L} \rho \\ \text{s.t.} &(31), (32) \end{aligned} \quad (33)$$

The design procedure of the optimal H_∞ observer-based feedforward-linearized PID FTC scheme for the agent (12) is organized as follows.

- 1) Apply the feedforward control in (9) to obtain the linearized system (17)
- 2) Construct the smoothing signal models (18) for the actuator fault $f_1(t)$ and sensor fault $f_2(t)$. Embed into the linearized system (17) to get the augment system (23).
- 3) Solve the LMIs-constrained optimization problem (33) by the two-step design to obtain the control gain K and observer gain $L = P_2^{-1}Y_2$.

Although the control gain and observer gain can already be found through the previous steps, the calculation speed of solving the matrix inequality (27) and the online calculation speed of controller and observer can be further improved by reducing the dimensionality. Observing the matrices A, B, C, B_2 in the linearized system (17), it can be further split into n subsystems if the matrices C, B_2 in the output equation (16) have the same form to A, B and $l = l_0 n, o = o_0 n$, i.e., $C = C_0 \otimes I_n, B_2 = B_{2,0} \otimes I_n$ where $C_0 \in \mathbb{R}^{l_0 \times 3}, B_{2,0} \in \mathbb{R}^{l_0 \times o_0}$. Let us decompose the PID tracking error $e(t) = \sum_{i=1}^n e_i(t) \otimes \mathbf{e}_i$, the control $u_{fb,i}(t) = \sum_{i=1}^n u_{fb,i}(t) \otimes \mathbf{e}_i$, the acuaor fault $f_{1,i}(t) = \sum_{i=1}^n f_{1,i}(t) \otimes \mathbf{e}_i$, the output $y(t) = \sum_{i=1}^n y_i(t) \otimes \mathbf{e}_i$, and the sensor fault $f_{2,i}(t) = \sum_{i=1}^n f_{2,i}(t) \otimes \mathbf{e}_i$ where $\mathbf{e}_i(t) \in \mathbb{R}^3, u_{fb,i}(t) \in \mathbb{R}^1, f_{1,i}(t) \in \mathbb{R}^1, y_i(t) \in \mathbb{R}^{l_0}, f_{2,i}(t) \in \mathbb{R}^{o_0}$ and \mathbf{e}_i is standard unit column vectors in \mathbb{R}^n , we get the n subsystems:

$$\begin{aligned} \dot{e}_i(t) &= A_0 e_i(t) + B_0(u_{fb,i}(t) + f_{1,i}(t)) \\ y_i(t) &= C_0 e_i(t) + B_{2,0} f_{2,i}(t) \end{aligned} \quad (34)$$

Remark 5: If the linearized system (17) can be split into n subsystems, this means that $\mathbf{e}_i(t)$, the PID error of each state variable $x(t)$ of agent in (8), can be measured independently via sensors to obtain the independent outputs $y_i(t)$. In actual systems, this is usually done.

By Theorem 1 again, the form shows that we can find the control gain $K_i \in \mathbb{R}^{1 \times s}$ and observer gain $L_i \in \mathbb{R}^{s \times l_0}$ of i th subsystem (34) that achieve the H_∞ observer-based stabilized control performance with prescribed attenuation level ρ_i , where $s = 3 + (k - 1) + (k - 1)o_0$. The origin control gain K of the origin agent system can be reconstructed by $K = [v_1 \ v_2 \ \dots \ v_n]^T$, $v_i = K_i^T \otimes \mathbf{e}_i$. The origin observer gain L can be reconstructed in the same way.

In this case, the calculation speed of finding gains K, L can be improved since the dimensionality is decrease. Furthermore, the online calculation speed of controller and observer can be also improved since there are more zeros in the gains K, L found by this method while maintaining robustness. More clearly, the number of elements in matrix K , i.e., the number of scalar gains, changes from $n \times sn$ to $n(1 \times s)$. For L , it changes from $sn \times l_0 n$ to $n(s \times l_0)$. The number of scalar gains to be designed between them is n times different.

Even though the design of the agent controller and observer has been completed, the trajectory design of UAV is not done yet. Since the UAV is an underactuated system, the "virtual" control input for UAV $u(t) = [f_x \ f_y \ f_z \ \tau_x \ \tau_y \ \tau_z]^T \in \mathbb{R}^6$ obtained from Theorem 1 needs to convert to actual control input $u'(t) = [F \ \tau_x \ \tau_y \ \tau_z]^T \in \mathbb{R}^4$. At the same time, the extra two degrees of freedom are used to find the remaining two reference trajectories ϕ_r and θ_r through inverse dynamics. That is to say, we want to find a total force F and its angles ϕ_r, θ_r and ψ_r from the three component forces f_x, f_y and f_z . By substituting $\Theta = \begin{bmatrix} \phi_r \\ \theta_r \\ \psi_r \end{bmatrix}$ into $\begin{bmatrix} f_x \\ f_y \\ f_z \end{bmatrix} = R(\Theta) \begin{bmatrix} 0 \\ 0 \\ F \end{bmatrix}$ from UAV dynamics in (3), the 3 unknown variables F, ϕ_r and θ_r can be found from these 3 equations because f_x, f_y, f_z and ψ_r are given.

The overall flowchart of tracking control is shown in Fig. 5. The reference generator is used to compute the actual reference trajectory $r(t)$ and control input $u(t)$ according to the output of local motion planning block $r'(t)$ and Theorem 1 $u'(t)$. The reference generator for robot is an identity function since it is a fully actuated system. Passing $r(t)$ through the integrator and differentiator, we get $\dot{r}(t)$. $\dot{r}(t)$ then pass to observer to calculate the PID tracking error $\mathbf{e}(t)$. Its differential, $\ddot{r}(t)$, then input to controller for feedforward control. The sensor measure not only the agent's own information (e.g., position or velocity) but environmental information. The former, measurement output $y(t)$, is passed to observer to get the estimation $\hat{\mathbf{e}}(t)$ for feedback control. The latter is passed back to the high-level block for positioning, mapping and object recognition.

V. SIMULATION RESULTS

In this section, a specific S&R procedure for URTS is given to illustrate the proposed UTRS system architecture and demonstrate the effectiveness of motion planning and control strategy. First, a S&R area divided into N_T areas, $area_i, i = 1, 2, \dots, N_T$, is given as shown in Fig. 6. To simplify the description, we will focus on the UAV and robot in i th team. Suppose each team has 5 agents, i.e., $N_A = 5$, then we can denote i th team as a set, $team_i = \{\alpha_{i,j}|i = 1, 2, \dots, 5\}$. At the beginning, the agents in $team_i$ are assigned the search tasks of $area_i$ to build the occupancy map and find goals. The search task is assumed to be obtained by dividing the unsearched region as shown in Fig. 7. Representing the search tasks as a set, $task_1 = \{T_j|j = 1, 2, \dots, 5\}$, then the proper agent-task pairs can be obtained through the task allocation block, $allocation_1 = \{(\alpha_{i,j}, T_j)|j = 1, 2, \dots, 5\}$. Suppose a goal is found after a while as shown in Fig. 7, at this point, we have a rescue task T_6 . The new task list $task_2 = task_1 \cup \{T_6\}$ is obtained by updating the old one. If the ground station assigns $\alpha_{i,5}$ and $\alpha_{i+1,2}$ to perform T_6 through the task allocation algorithm, then we have the new allocation $allocation_2 = (allocation_1 - \{(\alpha_{i,5}, T_2), (\alpha_{i+1,2}, T_3)\}) \cup \{(\alpha_{i,5}, T_6), (\alpha_{i+1,2}, T_6)\}$. Until the S&R mission is over, the task allocation block will continuously work in the similar way.

To explain the path planning block and behavior layer block, we choose the pairs $(\alpha_{i,5}, T_6)$ and $(\alpha_{i,1}, T_1)$ as example. For the robot $\alpha_{i,5}$, we have the goal configuration q_{goal} from the task T_6 . With the current configuration q_{start} and configuration space \mathcal{C} obtained by SLAM, the path $(\sigma_n), n \in \mathbb{Z} \cap [1, k_f], k_f = 27$ can be found as shown in Fig. 8. The behavior sequence (β_n) is set as $\beta_n = walking$ for $n \in \mathbb{Z} \cap [1, 5]$, $\beta_n = climbing$ for $n \in \mathbb{Z} \cap [6, 15]$ and $\beta_n = running$ for $n \in \mathbb{Z} \cap [16, 27]$. We choose the walking behavior to illustrate the local motion planning block of robots.

For the UAV $\alpha_{i,1}$, the path $(\sigma_n), n \in \mathbb{Z} \cap [1, k_f], k_f = 9$ is directly assigned as shown in Fig. 9 without going through path planning by Assumption 2.4. The behavior sequence (β_n) is set as $\beta_n = flying, n \in \mathbb{Z} \cap [1, 9]$.

Following the procedure in Fig. 4, the results of local motion planning of UAV flying and robot walking are shown in Fig. 9 and 10.

Through the previous steps, the reference trajectory $r(t)$ of flying and walking has been designed. The remaining parameters are set as follow.

Agents:

- 1) system parameters: Initial value $\tilde{x}(0) = [\mathbf{e}(0)^T, F_1(0)^T, F_2(0)^T, \tilde{e}(0)]^T = [[0.1X, \dots, 0.1X]^T, 0, 0, 0]^T$ where $X \sim \mathcal{N}(0, 1)$. $C_0 = I_3$.
- 2) designed parameters: $\rho = 30$. Actuator and sensor smoothing signal model window sizes are 3 and 4, respectively.

UAVs:

- 1) system parameters: $B_{2,0} = [0, 0.1, 1]^T, g = 9.81, m =$

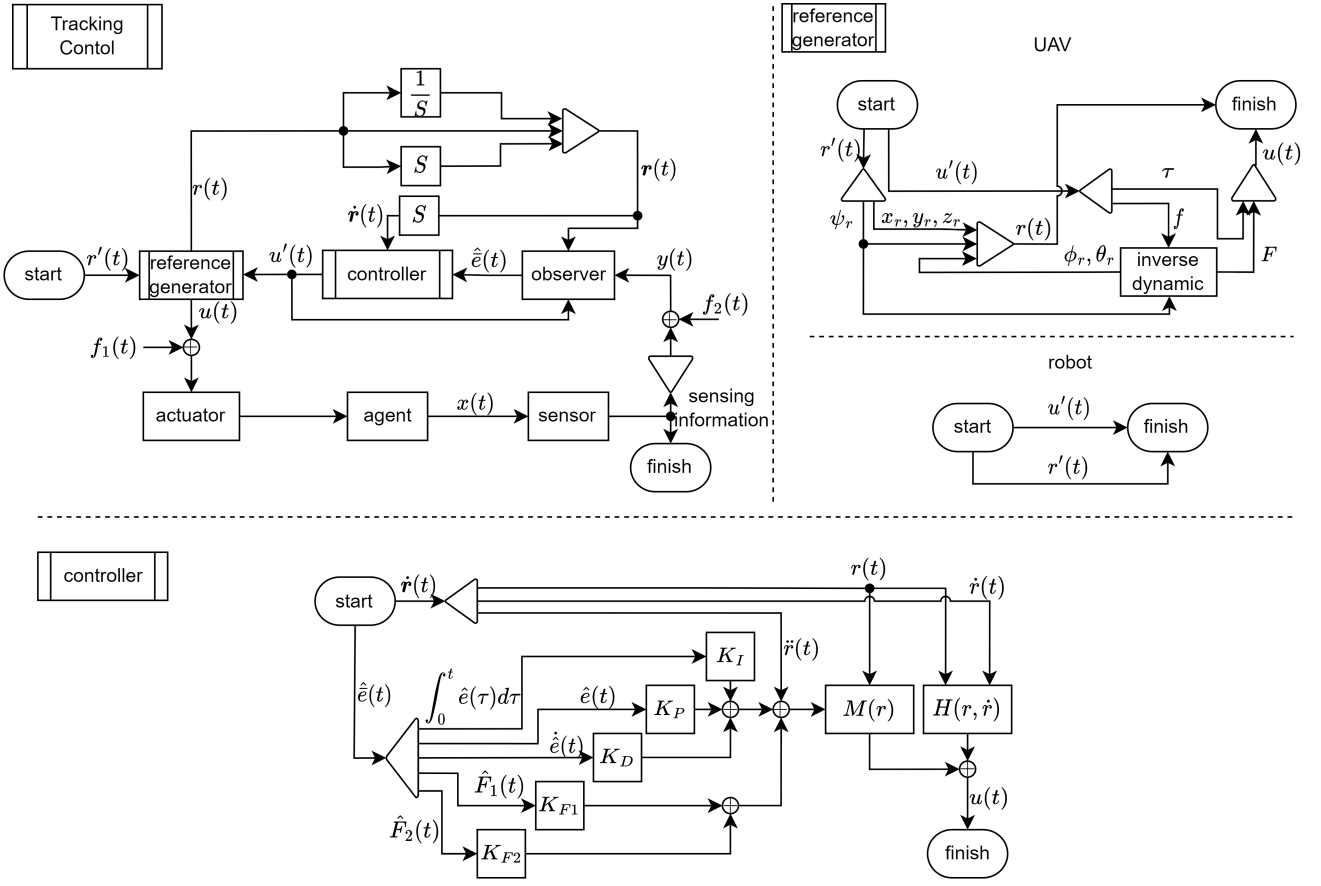


FIGURE 5: The flowchart of tracking control. The control scheme of UAV and robot is only different from the block, reference generator. The reason is that the underactuated nature of the UAV imposes the limitation on the control input and reference trajectory. By introducing this block, a general feedforward-linearized PID FTC for an agent in URTS is proposed.

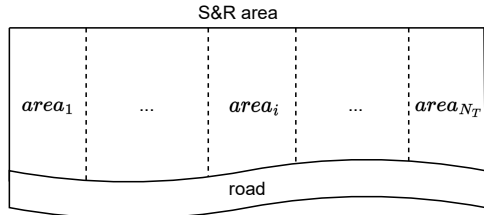


FIGURE 6: An example of a S&R area in URTS. This area is divided into N_T areas, and $team_i$ is responsible for $area_i$

- $2, J_x = J_y = 1.25, J_z = 2.2, K_x = K_y = K_z = 0.01, K_\phi = K_\theta = K_\psi = 0.012.$
- 2) designed parameters: $Q_1 = 10diag(diag(1, 100, 10), 0, 0, 0)$, $Q_2 = diag(0.1diag([1, 100, 10]), diag(1, 0.1, 0.01), 20diag(1, 0.1, 0.01, 0.001))$, $R = 0.02$.

Robots:

- 1) system parameters: Appendix E in [20]. $B_{2,0} = [0, 0, 1]^T$.
- 2) designed parameters: $Q_1 = 50diag(diag(1, 100, 10), 0, 0)$, $Q_2 = 5diag(diag([1, 100, 10]), diag(1, 0.1, 0.01), diag(1, 0.1, 0.01, 0.001))$, $R = 0.002$.

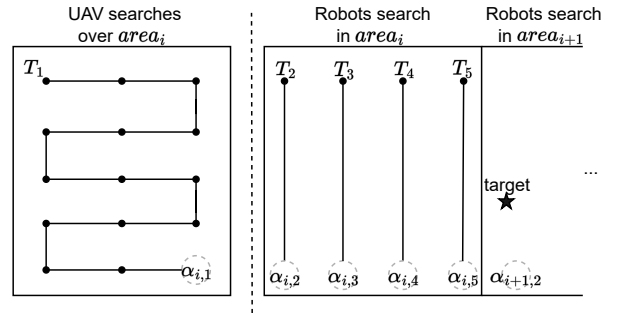


FIGURE 7: The search tasks in i th team at the begining. The search tasks $T_j, j = 1, 2, \dots, 5$ are to reach some consecutive destinations q_{goal} (black dots in figure). For robots, q_{goal} will be passed to path planning block to find collision-free paths (σ_n) . For UAV, the sequence formed by q_{goal} is directly the path (σ_n) due to the no-collision assumption.

The simulation results of tracking and estimation in tracking control block of the UAV $\alpha_{i,1}$ and the robot $\alpha_{i,2}$ are given as follow.

UAV: The trajectories of reference, state and estimated

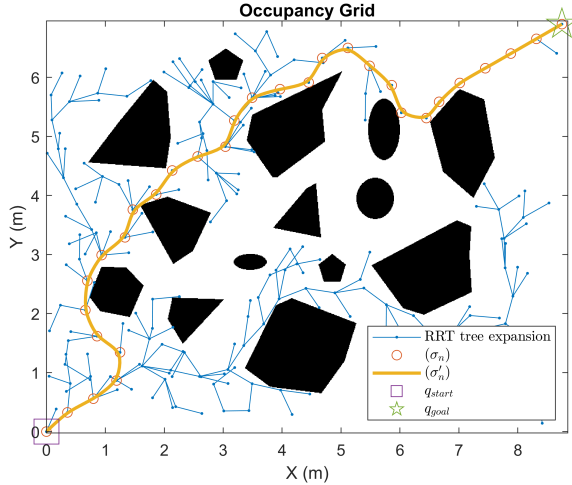


FIGURE 8: The path planning result of robot using RRT algorithm. The block polygons represent the obstacle space \mathcal{C}_{obs} .

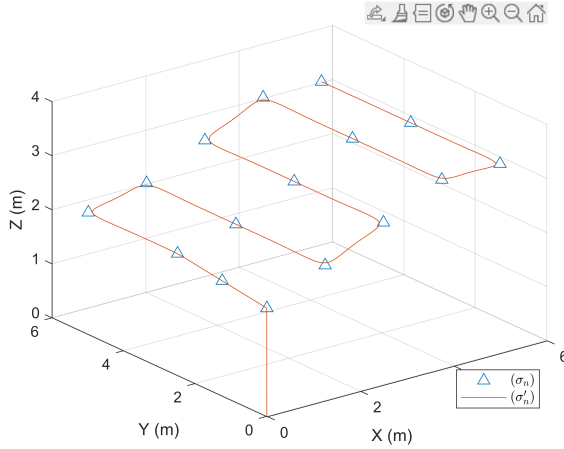


FIGURE 9: The result of local motion planning of UAV flying.

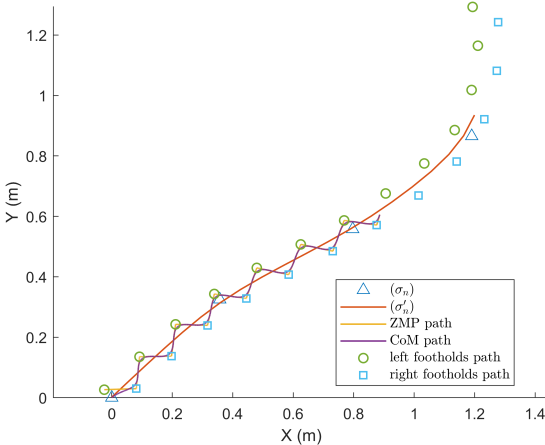


FIGURE 10: The top view of result of local motion planning of robot walking. The joint path, i.e., reference path $r[k]$ will be obtained by solving IK with CoM, left foothold and right foothold path.

state are shown in Fig. 11. The estimation of actuator fault $f_1(t) \in \mathbb{R}^6$ is shown in Fig. 12 where the disturbance $d_1(t)$ in $f_1(t)$ is set as $d_1(t) = [100 \sin(3t), \dots, 10 \sin(3t)]^T + \sum_{k=1, k \neq i}^{N_T} h_{i,1,k}(x_{i,1}(t))x_{k,1}(t)$, i.e., the non-couple term and the couple term in (10). Let $x_{i,1}(t) = [x_{i,1,1}(t), \dots, x_{i,1,6}(t)]^T$, then $h_{i,1,k}(x_{i,1}(t)) = \text{diag}(x_{i,1,1}(t), \dots, x_{i,1,12}(t))$. The estimation of sensor fault $f_2(t)$ is shown in Fig. 13 where $f_2(t)$ is set as a smoothed square wave as shown in figure. The control effort is shown in Fig. 14.

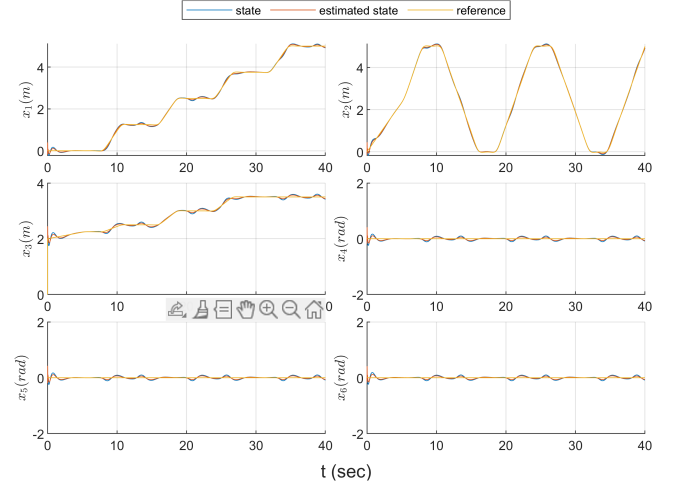


FIGURE 11: The trajectories of reference, state and estimated state of the UAV $\alpha_{i,1}$

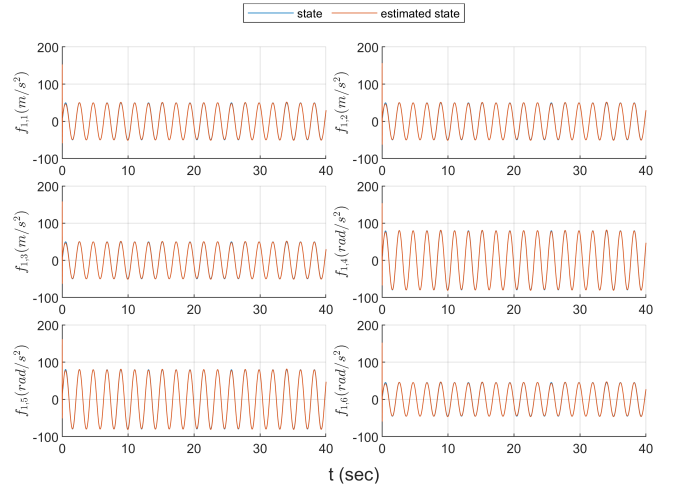
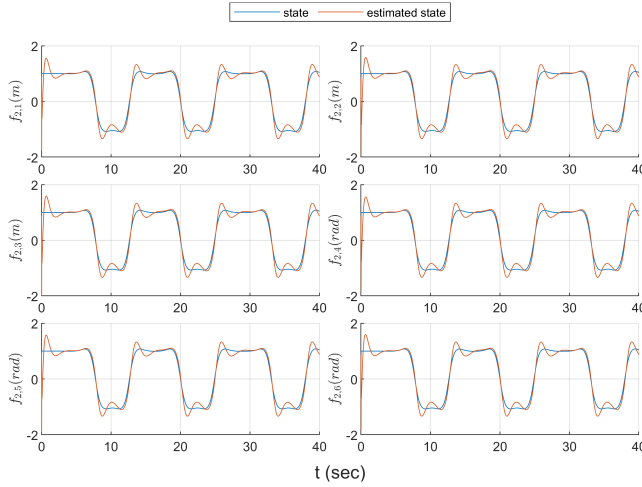
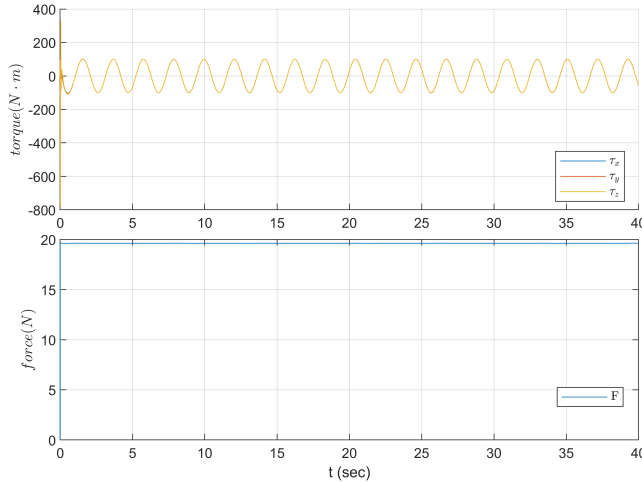


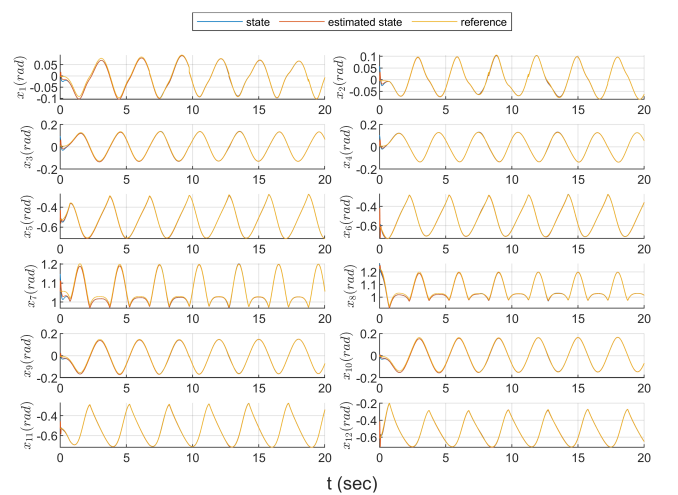
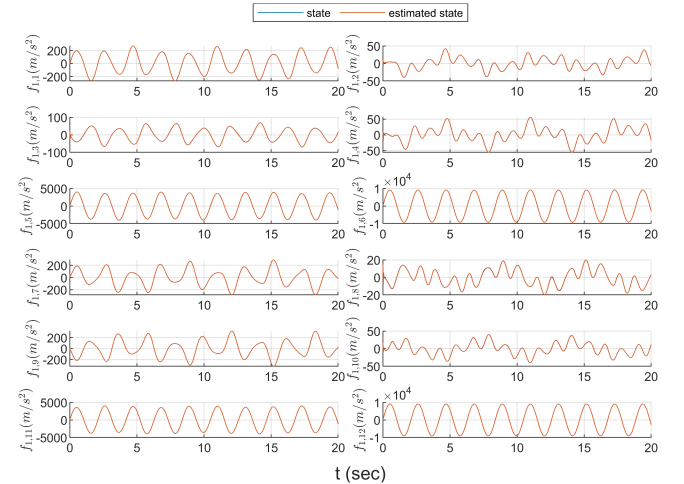
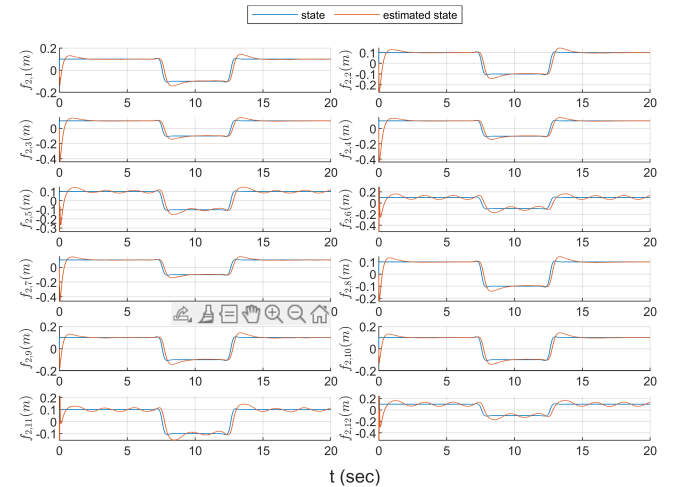
FIGURE 12: The estimation of actuator fault of the UAV $\alpha_{i,1}$

Robot: The trajectories of reference, state and estimated state are shown in Fig. 15. The estimation of actuator fault $f_1(t) \in \mathbb{R}^{12}$ is shown in Fig. 16 where the disturbance $d_1(t)$ in $f_1(t)$ is set as $d_1(t) = [10 \sin(3t), \dots, 10 \sin(3t)]^T + \sum_{k=1, k \neq j'}^{N_A} h_{i,j',k}(x_{i,j'}(t))x_{k,k}(t)$, i.e., the non-couple term and the couple term in (11). Let $x_{i,j'}(t) = [x_{i,j',1}(t), \dots, x_{i,j',12}(t)]^T$, then $h_{i,j',k}(x_{i,j'}(t)) = \text{diag}(x_{i,j',1}(t), \dots, x_{i,j',12}(t))$.

FIGURE 13: The estimation of sensor fault of the UAV $\alpha_{i,1}$ FIGURE 14: The control effort of the UAV $\alpha_{i,1}$

The estimation of actuator fault $f_1(t)$ is shown in Fig. 16 where the disturbance $d_1(t)$ in $f_1(t)$ is set as $d_1(t) = \sin(3t)$. The estimation of sensor fault $f_2(t)$ is shown in Fig. 17 where $f_2(t)$ is set as a smoothed square wave as shown in figure. The control effort is shown in Fig. 18

In Fig. 11, the tracking and estimation errors of UAV position and attitude reach steady state within 2 second. There is a brief jitter when the sensor fault signal changes drastically, but it returns quickly to steady state. In Fig. 15, the tracking and estimation errors of robot joint angles immediately reach and maintain steady under the influence of fault signals. In Fig 12 and 16, the results show that the actuator fault, i.e., disturbances and feedforward errors, can be effectively estimated. However, in Fig 13 and 17, the estimation of sensor fault has an overshoot phenomenon when there is a large change and returns to a steady state after about 3 seconds. In Fig 14 and 18, the control efforts has high frequency and high amplitude performance at the initial instance due to the high gain characteristic of the robust control. After that, they maintain the sine wave shape to offset

FIGURE 15: The trajectories of reference, state and estimated state of the robot $\alpha_{i,2}$ FIGURE 16: The estimation of actuator fault of the robot $\alpha_{i,2}$ FIGURE 17: The estimation of sensor fault of the robot $\alpha_{i,2}$

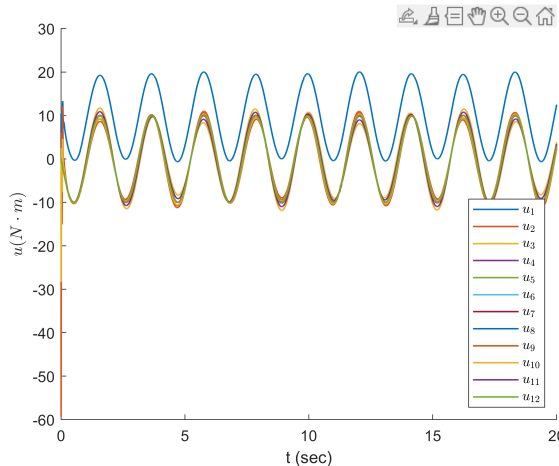


FIGURE 18: The control effort of the robot $\alpha_{i,2}$

the estimated actuator fault value. Besides, it can be seen that the total force F remains constant against gravity in Fig 14.

For further verification, we visualized the simulation of a team in URTS and the configuration trajectory of biped robot on the online resource (cite:online source). The results again demonstrate the effectiveness of the proposed method.

VI. CONCLUSION

In this study, a system architecture of URTS for R&S usage is given. This gives a holistic view of the operational framework for UTRS. Next, we focus on part of the system architecture of UTRS, i.e., the reference trajectory design of UAV flying and robot walking and controller design of UAV and robot. The procedure of reference trajectory design method of UAV flying and robot walking is also given in detail. A robust H_∞ decentralized observer-based feedforward-linearized PID FTC strategy is proposed to control the agents in URTS under the external disturbances. The control problem of UAV and robot are solved together via a transformation from a general agent model. After analysis, the control problem is further transformed into a LMI-constrained optimization problem. Through two-step design procedure, the problem is effectively solved by MATLAB LMI Toolbox. The simulation results give an example of the proposed URTS architecture to more concretely illustrate its operational flow. Finally, the effectiveness of the designed controller and observer is also verified by the simulation results. In the future, we will...

REFERENCES

- [1] Laurent Kloeker, Tobias Moers, Lennart Vater, Adrian Zlocki, and Lutz Eckstein. Utilization and potentials of unmanned aerial vehicles (uavs) in the field of automated driving: A survey. In 2021 5th International Conference on Vision, Image and Signal Processing (ICVISP), pages 9–17, 2021.
- [2] Ali Dorri, Salil S. Kanhere, and Raja Jurdak. Multi-agent systems: A survey. IEEE Access, 6:28573–28593, 2018.
- [3] Fei Chen, Wei Ren, et al. On the control of multi-agent systems: A survey. Foundations and Trends® in Systems and Control, 6(4):339–499, 2019.
- [4] Wanglei Cheng, Ke Zhang, Bin Jiang, and Steven X. Ding. Fixed-time fault-tolerant formation control for heterogeneous multi-agent systems with parameter uncertainties and disturbances. IEEE Transactions on Circuits and Systems I: Regular Papers, 68(5):2121–2133, 2021.
- [5] George Marios Skaltsis, Hyo-Sang Shin, and Antonios Tsourdos. A survey of task allocation techniques in mas. In 2021 International Conference on Unmanned Aircraft Systems (ICUAS), pages 488–497, 2021.
- [6] Han-ye Zhang, Wei-ming Lin, and Ai-xia Chen. Path planning for the mobile robot: A review. Symmetry, 10(10):450, 2018.
- [7] Jawad N. Yasin, Sherif A. S. Mohamed, Mohammad-Hashem Haghbayan, Jukka Heikkonen, Hannu Tenhunen, and Juha Plosila. Unmanned aerial vehicles (uavs): Collision avoidance systems and approaches. IEEE Access, 8:105139–105155, 2020.
- [8] Barbara Arbanas, Antun Ivanovic, Marko Car, Matko Orsag, Tamara Petrovic, and Stjepan Bogdan. Decentralized planning and control for uav-ugv cooperative teams. Autonomous Robots, 42(8):1601–1618, 2018.
- [9] Linjun Li, Yinglong Miao, Ahmed H. Qureshi, and Michael C. Yip. Mpc-mpnet: Model-predictive motion planning networks for fast, near-optimal planning under kinodynamic constraints. IEEE Robotics and Automation Letters, 6(3):4496–4503, 2021.
- [10] Tolga Olcay and Ahmet Özkurt. Design and walking pattern generation of a biped robot. Turkish Journal of Electrical Engineering and Computer Sciences, 25(2):761–769, 2017.
- [11] Yassine Sabri, Najib El Kamoun, and Fatima Lakrami. A survey: Centralized, decentralized, and distributed control scheme in smart grid systems. In 2019 7th Mediterranean Congress of Telecommunications (CMT), pages 1–11, 2019.
- [12] Chunping Wang, Jiaqi Wang, Ping Wu, and Jinfeng Gao. Consensus problem and formation control for heterogeneous multi-agent systems with switching topologies. Electronics, 11(16):2598, 2022.
- [13] Damiano Rotondo, Fatiha Nejjari, and Vicenç Puig. Passive and active ftc comparison for polytopic lpv systems. In 2013 European Control Conference (ECC), pages 2951–2956, 2013.
- [14] Brian Paden, Michal Cáp, Sze Zheng Yong, Dmitry Yershov, and Emilio Frazzoli. A survey of motion planning and control techniques for self-driving urban vehicles. IEEE Transactions on intelligent vehicles, 1(1):33–55, 2016.
- [15] Alaa Khamis, Ahmed Hussein, and Ahmed Elmogy. Multi-robot Task Allocation: A Review of the State-of-the-Art, pages 31–51. Springer International Publishing, Cham, 2015.
- [16] Mohamed Elbanhawi and Milan Simic. Sampling-based robot motion planning: A review. Ieee access, 2:56–77, 2014.
- [17] Yuanchang Liu and Richard Bucknall. A survey of formation control and motion planning of multiple unmanned vehicles. Robotica, 36(7):1019–1047, 2018.
- [18] Jingjin Yu and Steven M LaValle. Multi-agent path planning and network flow. In Algorithmic foundations of robotics X, pages 157–173. Springer, 2013.
- [19] Francesco Sabatino. Quadrotor control: modeling, nonlinearcontrol design, and simulation, 2015.
- [20] M.Y.Lee B.S.Chen, Y.Y.Tsai. online supplementary file. <https://www.dropbox.com/s/qiv63y5hw7vrubp/SupplementFileRobot.pdf>.
- [21] Shuuji Kajita, Osamu Matsumoto, and Muneharu Saigo. Real-time 3d walking pattern generation for a biped robot with telescopic legs. In Proceedings 2001 ICRA. IEEE international conference on robotics and automation (Cat. no. 01ch37164), volume 3, pages 2299–2306. IEEE, 2001.
- [22] Qiang Huang, Kazuhito Yokoi, Shuuji Kajita, Kenji Kaneko, Hirohiko Arai, Noriho Koyachi, and Kazuo Tanie. Planning walking patterns for a biped robot. IEEE Transactions on robotics and automation, 17(3):280–289, 2001.
- [23] S. Kajita, F. Kanehiro, K. Kaneko, K. Fujiwara, K. Harada, K. Yokoi, and H. Hirukawa. Biped walking pattern generation by using preview control of zero-moment point. In 2003 IEEE International Conference on Robotics and Automation (Cat. No.03CH37422), volume 2, pages 1620–1626 vol.2, 2003.
- [24] Frank L Lewis, Draguna Vrabie, and Vassilis L Syrmos. Optimal control. John Wiley & Sons, 2012.
- [25] Bor-Sen Chen and Jun-Hao Lin. Robust collaborative team formation control of hybrid teams of biped robots and wheeled vehicles under external disturbance and communication interactions. IEEE Access, 10:77633–77657, 2022.
- [26] Jun Yang, Cunjia Liu, Matthew Coombes, Yunda Yan, and Wen-Hua Chen. Optimal path following for small fixed-wing uavs under wind disturbances. IEEE Transactions on Control Systems Technology, 29(3):996–1008, 2021.

- [27] Bor-Sen Chen, Chia-Chou Wu, and Yen-Wen Chen. Human walking gait with 11-dof humanoid robot through robust neural fuzzy networks tracking control. *International Journal of Fuzzy Systems*, 15(1), 2013.
- [28] Bor-Sen Chen, Min-Yen Lee, Wei-Yu Chen, and Weihai Zhang. Reverse-order multi-objective evolution algorithm for multi-objective observer-based fault-tolerant control of t-s fuzzy systems. *IEEE Access*, 9:1556–1574, 2021.
- [29] Stephen Boyd, Laurent El Ghaoui, Eric Feron, and Venkataramanan Balakrishnan. Linear matrix inequalities in system and control theory. SIAM, 1994.

• • •